

CO adsorption over Pd nanoparticles: a general framework for IR simulations on nanoparticles

Constantinos D. Zeinalipour-Yazdi^{†,‡,*}, David J. Willock^{†,*}, Liam Thomas[†], Karen Wilson[‡] and Adam F. Lee^{‡,*}

[†] Cardiff Catalysis Institute, Cardiff University, Park Place, Cardiff CF10 3AT, UK

[‡] Department of Chemistry, University College London, London, WC1H 0AJ, UK

[‡] European Bioenergy Research Institute, Aston University, Birmingham, B4 7ET, UK

KEYWORDS: *Palladium; Nanoparticles; Carbon monoxide; Density functional theory; Chemisorption; IR spectroscopy*

ABSTRACT: CO vibrational spectra over catalytic nanoparticles under high coverages/pressures are discussed from a DFT perspective. Hybrid B3LYP and PBE DFT calculations of CO chemisorbed over Pd₄ and Pd₁₃ nanoclusters, and a 1.1 nm Pd₃₈ nanoparticle, have been performed in order to simulate the corresponding coverage dependent infrared (IR) absorption spectra, and hence provide a quantitative foundation for the interpretation of experimental IR spectra of CO over Pd nanocatalysts. B3LYP simulated IR intensities are used to quantify site occupation numbers through comparison with experimental DRIFTS spectra, allowing an atomistic model of CO surface coverage to be created. DFT adsorption energetics for low CO coverage ($\theta \rightarrow 0$) suggest the CO binding strength follows the order hollow > bridge > linear, even for dispersion-corrected functionals for sub-nanometer Pd nanoclusters. For a Pd₃₈ nanoparticle, hollow and bridge-bound are energetically similar (hollow \approx bridge > atop). It is well known that this ordering has not been found at the high coverages used experimentally, wherein atop CO has a much higher population than observed over Pd(111), confirmed by our DRIFTS spectra for Pd nanoparticles supported on a KIT-6 silica, and hence site populations were calculated through a comparison of DFT and spectroscopic data. At high CO coverage ($\theta = 1$), all three adsorbed CO species co-exist on Pd₃₈, and their interdiffusion is thermally feasible at STP. Under such high surface coverages, DFT predicts that bridge-bound CO chains are thermodynamically stable and isoenergetic to an entirely hollow bound Pd/CO system. The Pd₃₈ nanoparticle undergoes a linear (3.5 %), isotropic expansion with increasing CO coverage, accompanied by 63 and 30 cm⁻¹ blue-shifts of hollow and linear bound CO respectively.

1. Introduction

CO adsorption and activation over platinum group metals (PGMs, *i.e.* Pt, Ir, Ru, Rh, and Pd) [1] are key steps in some of the world's most important catalytic processes [2, 3]. Early surface science studies by Ertl and co-workers shed valuable light on CO adsorption/oxidation (*i.e.* $\text{CO} + \frac{1}{2}\text{O}_2 \rightarrow \text{CO}_2$) on palladium surfaces, evidencing a competitive Langmuir–Hinshelwood mechanism [4-8]. Nowadays, palladium is a key component of automotive emission control three-way catalysts (TWCs) for gasoline vehicles, facilitating low temperature oxidation [9]. Supported PGMs have also shown outstanding low temperature performance for the water-gas shift (WGS) reaction (*i.e.* $\text{CO} + \text{H}_2\text{O} \rightarrow \text{CO}_2 + \text{H}_2$) [10], the electrochemical oxidation of CO [11], and CO methanation in which CO coverage-dependent rate changes of 2-3 orders of magnitude have been recently observed [12]. These important processes place a heavy demand on the supply of these costly and scarce elements. To mitigate the cost and improve the sustainability of PGM catalysts, academic and industrial researchers seek more efficient catalyst designs, such as supported nanoparticles (NPs), which offer very high surface area to volume ratios for the active metal component, or alloying with a non-noble metal to minimise the precious metal content and tailor its electronic properties [13]. A strong NP/support interaction is also desirable to hinder particle sintering and attendant loss of active surface area.

In addition to its roles in pollution control and chemical synthesis, CO is also widely employed in heterogeneous catalysis as a strongly-interacting probe molecule for evaluating the dispersion and morphology of PGM nanoparticles via thermal desorption and/or vibrational spectroscopies [14, 15]. However, the correct interpretation of resulting experimental spectra is critically dependent upon a quantitative understanding of factors influencing the observed CO stretching frequency, which to date has only been derived via surface science experiments over well-defined single crystal surfaces. For nanoparticulate catalysts such CO stretching frequencies are anticipated to be sensitive to NP size, the exposed facets, support interactions, and coverage dependent (substrate-mediated or direct) lateral interactions between co-adsorbed CO molecules: these effects are extremely difficult to probe independently through experiment. Density functional theory (DFT) calculations offer a powerful methodology by which to estimate the energetic, structural and spectroscopic properties of CO over free and supported transition and noble metal clusters [16-21] and oxides [22]. We have therefore undertaken the first systematic DFT level calculations, and associated IR spectral simulations, of CO over a family of related, isolated Pd clusters seeking to quantify the influence of particle size and CO coverage based only on the intrinsic properties of the metal NPs. The resulting calculations offer valuable insight into the fundamental processes that occur during CO adsorption over metal NPs under 'real world' conditions of high coverage and/or pressure [16].

CO adsorption on Pd surfaces and NPs has been investigated by both experiment and theory [4, 23-26]. Early photoelectron diffraction experiments showed that at low coverage ($\theta = 0.1 - 0.5$) CO preferentially adsorbs at three-fold

hollow sites on Pd(111) [27]. At higher coverage ($\theta = 0.6 - 0.7$) the preference switches to bridge sites, with atop species only appearing at very high surface densities ($\theta = 0.75$) [28]. Goodman and co-workers examined CO adsorption over Pd(111) and Pd(100) [29] single crystals at low and high coverage via temperature programmed desorption (TPD) and surface IR spectroscopy (RAIRS), uncovering a correlation between the activation energies for desorption and corresponding rates of CO oxidation. For Pd NPs, Wolter et al performed a systematic study of CO over Pd/Al₂O₃/NiAl(100). A strong atop signal was observed by RAIRS for small NPs (10-50 atoms), in addition to a contribution from bridge sites which becomes more important for larger particles. Upon heating, atop CO desorbed first leaving only bridge-bound molecules >335 K for 300 atom NPs. Dropsch and Baerns also studied CO adsorption on oxide supported Pd NPs by microcalorimetry and TPD [30], concluding that bridge-bound CO dominated at low coverages ($\theta < 0.4$), whereas three distinct CO species were observed at higher coverage. The size-dependence of CO adsorption on Pd NPs (120-4900 Pd atoms) supported over Fe₃O₄/Pt(111) was also explored by single-crystal microcalorimetry [31, 32]; a 20-40 kJ.mol⁻¹ decrease in adsorption energy was noted with CO coverage, similar to that predicted by DFT calculations for a Rh₄ nanocluster [16].

CO adsorption energetics have been extensively investigated by DFT over various transition and noble metal surfaces [33, 34] and clusters [17, 35]. In particular, it has been found that the site preference for CO adsorption on Pt(111) is incorrectly predicted by DFT methods, with predictions favouring high co-ordination CO adsorption sites over low co-ordination sites [34]. For Pd(111), three fold hollow sites are also calculated to provide the lowest adsorption energy for single CO molecules [36, 37] although this is in agreement with STM, LEED [38] and SFG [25, 39] studies. Rösch and coworkers recently calculated the size-dependent adsorption energy of CO on 13-116 atom Pd NPs [40, 41] for various low coverage structures, identifying 50-100 atom clusters as the optimum to minimise CO adsorption, although this finding may have been influenced by the choice of the simple LDA functional, particularly in the light of recent microcalorimetric data from Schauermaun and co-workers which evidenced a decrease in adsorption energy with NP size [31].

Here we investigate the impact of Pd NP size and CO coverage on the energetics of CO adsorption, with a view to establishing a general framework within DFT for accurately simulating the IR vibrational spectra of CO over palladium nanoparticulate catalysts. Such a theoretical basis will aid the interpretation of experimental IR spectra in respect of the nature, number density, and adsorption strength of different CO species bound to practical catalysts, and hence enhance the utility of IR spectroscopies (DRIFTS, ATR-IR and RAIRS) routinely employed to determine the morphology and electronic structure of practical PGM catalysts [18, 42]. We find that structural (e.g. average Pd-Pd and C-O bond lengths), energetic (e.g. CO adsorption enthalpy) and spectroscopic properties (e.g. C-O stretching frequency and dipole) of the CO/Pd_n system evolve strongly with particle size and CO coverage. The coverage dependent heat of CO adsorption on Pd₃₈ NP and associated relative stability of different adsorption sites is also rationalised.

2. COMPUTATIONAL METHODS

Restricted and unrestricted DFT calculations were used, as implemented in Gaussian 09 [43], with the commonly used B3 exchange functional [44] combined with the LYP non-local correlation functional [45] (B3LYP). We also briefly tested other exchange-correlation (XC) functionals: M06-2X [46], TPSSh [47], LC-wPBE [48], PBE [49], B3PW91 [44, 50] (see supporting information, S-Fig. 1) which yielded the same relative total energy order for Pd₄(3,1) at various spin multiplicities (s.m.). We adopted a computational strategy whereby the structures of Pd₄(3,1) and Pd₁₃(3,7,3) clusters were first fully optimized at a UB3LYP/CEP-121G(Pd), aug-cc-pVTZ(C,O) level of theory, in order to identify the possible adsorption configurations (e.g. linear, bridge and hollow). This level of theory was found sufficient among basis sets/ECP of varying size, LanL2mb [51, 52], LanL2dz [52, 53], CEP-121G [54, 55], aug-cc-pVTZ [56-60] and QZVP [61, 62], to yield converged adsorption energies (ΔE_{ads}) to within a few kJ.mol⁻¹ of the basis set superposition error (BSSE) corrected adsorption energies (ΔE_{BSSE}) obtained by the counterpoise method of Boys and Bernardi [63]. In **Fig. 1** we show that the basis set/ECP CEP-121G(Pd),aug-cc-pVTZ(C,O) yields quantitatively similar results to the computationally intensive QZVP basis set that contains twice as many basis functions. Full optimization is critical [64] since strong adsorption-induced structural changes to the transition metal cluster were observed, especially for the Pd nanoclusters (i.e. Pd_{4,13}). Linear dependencies of the basis functions were removed by using the spherical version (5d and 7f) of these basis sets. The SCF convergence criteria for the root mean square (rms) density matrix and the total energy were respectively set to 10⁻⁸ e/bohr⁻³ and 10⁻⁶ Hartree.

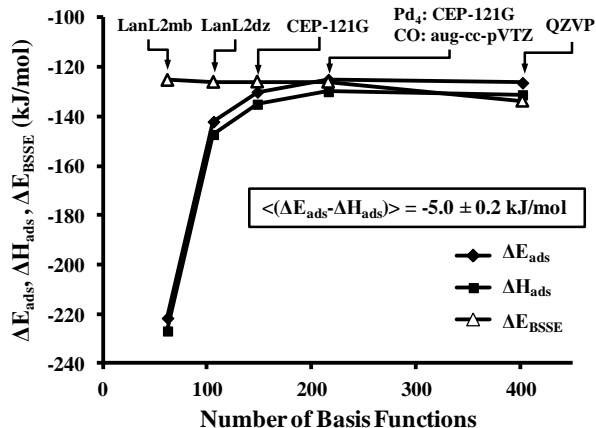


Figure 1. Adsorption energy, enthalpy and BSSE-corrected energy as a function of the number of basis functions for Pd₄-CO. Open shell calculations were also examined for spin contamination, which was found to be negligible.

Calculations for the larger Pd₃₈ NP were obtained via spin-polarized Γ point [65] calculations using VASP 5.3 [66, 67]. Exchange and correlation effects were considered within the generalized gradient approximation (GGA) using the Perdew-Burke-Ernzerhof [68] (PBE) XC functional, with the projector augmented-wave (PAW) method [69, 70] used to represent core states (1s for C and O, and 1s to 4p for Pd). The cut-off energy for plane-wave expansion was set to 500 eV. Nanoparticle/adsorbate models were centred within a 30 Å cubic box to ensure a sufficient vacuum gap around the cluster/adsorbate system. Geometry optimizations were performed with a residual force threshold of 0.015 eV.Å⁻¹ using the conjugate-gradient algorithm. Convergence criteria for the electronic relaxation during optimization (frequency) calculations were based on the change of energy between SCF cycles with a threshold of 10⁻⁴ eV (10⁻⁷ eV). The initial charge density was obtained by superposition of atomic charges, and the projection operators were evaluated in reciprocal space.

We note that, for metallic systems, the B3LYP functional is not regularly used due to its failure to recover the homogeneous electron gas solution for itinerant electron states in bulk metals [71]. For metal complexes the functional is quite widely used and a combined B3LYP/CCSD(T) study has appeared for cationic group 10 and group 11 carbonyl complexes [72]. The nanoclusters considered here are intermediate in size. We use the B3LYP functional only for its reliability in vibrational analysis including intensity estimates for the IR modes of CO on the smaller clusters. The total adsorption energy per CO molecule ($\Delta E_{\text{ads,CO}}$) was calculated using,

$$\Delta E_{\text{ads, CO}} = (E_{\text{Pd}_m(\text{CO})_n} - E_{\text{Pd}_m} - n_{\text{CO}} E_{\text{CO}}) / n_{\text{CO}}$$

where E_i is the total energy of fully optimized species i and n_{CO} the number of adsorbed CO molecules. Note that this definition means that negative adsorption energies are favourable compared to gas phase CO and a free nanoparticle. The surface coverage of CO has been defined based on the following equation

$$\theta_{\text{CO}} = n_{\text{CO}} / n_{\text{Pd,surf}}$$

where $n_{\text{Pd,surf}}$ is the number of surface Pd atoms of the NP. The vibrational frequencies were explicitly calculated by diagonalizing the Hessian matrix using the finite-difference (FD) method. Additional calculations using the density-functional-perturbation-theory (DFPT) method within VASP were used to ensure that agreement within 2 cm⁻¹ could be obtained with this computational protocol. The relative intensities of linear-CO (lCO), bridge (bCO) and three-fold (3f) hollow (hCO) species were calibrated against the results for tetrahedral (T_d) Pd₄(3,1) and cubooctahedral (O_h) Pd₁₃(3,7,3). Infrared spectra were simulated by fitting a Lorentzian function with a FWHM = 15 cm⁻¹, centred at each stretching frequency calculated from the FD method.

3. RESULTS AND DISCUSSION

3.1 Effect of NP size on CO adsorption. Previous computational [41, 64] and microcalorimetric [32] studies of CO adsorption on Pd NPs have suggested a strong cluster size-dependence. At low coverages, CO adsorption energies can vary by almost 100 kJ.mol⁻¹ (falling from -202 kJ.mol⁻¹ for Pd₁₃ to -109 kJ.mol⁻¹ for Pd₂₅), resulting in a critical cluster size (50-100 atoms) wherein CO adsorption is weakest [41]. Another microcalorimetry study showed that initial heats of adsorption that fall linearly with particle size from the Pd(111) surface value of 149 ± 3 kJ mol⁻¹ down to 106 ± 1 kJ mol⁻¹ for particles of 2 nm dimension [31]. Adsorption microcalorimetry offers precise adsorption heats [73, 74], but no direct insight, into CO

bonding modes. Atomistic simulations herein, provide adsorption energies of CO species according to their structural identification (i.e. lCO, bCO or hCO), however it is clear from the introductory discussion of site preference that this is likely to give insufficient accuracy to allow relative abundances ($n_{\text{lCO}}, n_{\text{bCO}}, n_{\text{hCO}}$) to be determined. However, DFT calculations can be used to interpret IR spectroscopic signatures of adsorbed CO species by obtaining the IR intensity factors as a function of CO position, and then using experimental data to interpret the site populations. IR intensity calculations are not currently available in VASP for these systems, and are most accurate using a hybrid functional method for which the computational expense increases rapidly with system size. Accordingly, we have performed calculations using small reference systems (Pd_4 and Pd_{13}), and extrapolated the results to the larger Pd_{38} cluster size. The choice of hybrid B3LYP functional for the calculation of IR oscillator frequencies was based on its earlier success in the spectral band assignment of diffuse reflectance infrared Fourier-Transform (DRIFT) spectra obtained for CO chemisorption over a highly dispersed $\text{Rh}/\gamma\text{-Al}_2\text{O}_3$ catalyst [18]. Due to computational cost, this method is limited to the smaller cluster sizes with single adsorbates. Therefore we additionally employed the more commonly used PBE functional for the largest cluster size, and to examine coverage effects.

Here, we briefly examine the dependence of CO adsorption energy on Pd cluster size, before considering the effect of CO surface coverage. The energetics of CO chemisorption were studied for three high symmetry Pd particles: tetrahedral $\text{Pd}_4(3,1)$ (0.4 nm), cubooctahedral $\text{Pd}_{13}(3,7,3)$ (0.8 nm) and cubooctahedral $\text{Pd}_{38}(\text{O}_h)$ (1.1 nm). Three distinct configurations were identified and are presented in **Fig. 2**: *linear* (lCO), *bridge* (bCO) and *hollow* (hCO) bound molecules, which resemble the stable adsorption configurations found over $\text{Rh}_4(3,1)$ [10, 17]. Additionally, di-carbonyl (di-CO) and tri-carbonyl species (tri-CO) were stable on Pd_4 but could not be identified on $\text{Pd}_{38}(\text{O}_h)$ and hence were not further considered. Calculated adsorption energies of CO at a low coverage ($\theta \rightarrow 0$) are given in **Table 1**. For all adsorption sites we observe a strong particle size-dependence in good agreement with earlier theoretical studies [32, 41, 64]: on Pd_4 $\Delta E_{\text{ads}} = -130$ to -257 $\text{kJ}\cdot\text{mol}^{-1}$; on Pd_{13} $\Delta E_{\text{ads}} = -167$ to -223 $\text{kJ}\cdot\text{mol}^{-1}$; and for Pd_{38} $\Delta E_{\text{ads}} = -161$ to -196 $\text{kJ}\cdot\text{mol}^{-1}$. Interestingly, this cluster size-dependence of CO adsorption energy was dependent on the adsorption configuration. For hollow and bridge-bound CO, $\Delta E_{\text{ads, CO}}$ indicates weaker binding with increasing NP size (0.4 nm \rightarrow 1.1 nm), whereas linear bound CO becomes more strongly bound. The calculated sensitivity of CO adsorption energy to NP size scales roughly with the coordination number (i.e. number of Pd-C bonds), such that $\text{hCO} > \text{bCO} > \text{lCO}$.

According to these results, the experimentally observed trend should then depend on the site occupancies for the three positions which may be influenced by sample pre-treatment. Campbell and co-workers [31] suggested that the experimentally observed weakening of adsorption could result from a Van der Waals dispersion effect, which would be expected to reduce with particle size. We have used the PBE-D2 method to test if dispersion energy is a significant factor and the results are presented in Table S1. The dispersion contribution to adsorption energies was small, and does not affect the observed trend with cluster size. The D2 correction is an atom-atom interaction model which does not include dispersion interactions with the delocalised electrons of a metal. Nevertheless, these calculations indicate that dispersion effects for CO on metals at low coverage are likely negligible. We speculate that the trend in adsorption energy with particle size reported by Campbell may be an indication that the hollow and bridge site populations were high in their experiments.

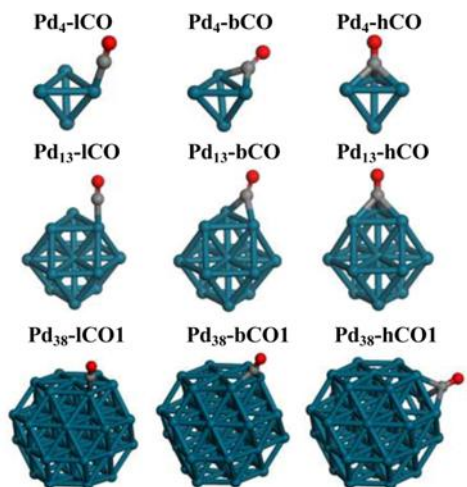


Figure 2. Structures for linear, bridge and three-fold (3f) hollow bound CO on $\text{Pd}_4(3,1)$, $\text{Pd}_{13}(3,7,3)$ and $\text{Pd}_{38}(\text{O}_h)$, respectively.

Table 1. Vibrational stretching frequency, intensity, bond length and adsorption energy of CO(g), and CO on Pd₄ and Pd₁₃ (B3LYP/CEP-121G(Pd),aug-cc-pVTZ(C,O)) and Pd₃₈ (PBE, planewaves, E_{cut} = 500 eV, 30Å cubic box), NPs respectively. The optimised structures of Pd₄, Pd₁₃ and Pd₃₈ had a s.m. of 3, 7 and 9, respectively (S-Fig. 1).

label	p.g. ^a	s.m. ^b	ν_{C-O} (cm ⁻¹)	I_{C-O}^b (10 ⁶ m mol ⁻¹)	r_{C-O}^b (Å)	ΔE_{ads} (kJ.mol ⁻¹)
Pd₄-lCO	C ₁	3	2102	1125	1.139	-130
Pd₄-bCO	C _{2v}	1	1879	587	1.171	-208
Pd₄-hCO	C _{3v}	1	1768	475	1.187	-257
Pd₁₃-lCO	C _s	3	2088	1396	1.142	-149
Pd₁₃-bCO	C _s	3	1931	955	1.161	-198
Pd₁₃-hCO	C _{3v}	3	1827	815	1.175	-200
Pd₃₈-lCO1	C _s	9 ^c	2058	-	1.150	-161
Pd₃₈-bCO1	C _s	9 ^c	1886	-	1.171	-189
Pd₃₈-hCO1	C _s	9 ^c	1786	-	1.185	-196
CO(g)	D _{∞h}	1	2131	-	1.133	-

^a p. g. = point group symmetry

^b s.m. = spin multiplicity = 2S + 1

^c spin-polarised calculation

In **Table 1**, the stretching frequency (ν_{C-O}), IR intensity (I_{C-O}), bondlength (r_{C-O}) are also presented for the various configurations. Data for Pd₄ and Pd₁₃ are at the B3LYP level with a localized basis set so that calculated IR intensities can be included. We note that a linear adsorption mode results in a larger transition dipole moment than either hollow or bridge sites. For the Pd₄ cluster, a singlet state was energetically favourable for the bridge and hollow adsorption modes, but for **Pd₄-lCO** and the bare Pd₄ cluster the triplet state is lower in energy, in agreement with an earlier study using B3LYP/LanL2dz [75] and detailed MCSCF studies of the low lying states of Pd₄ [76]. For Pd₁₃, we find the triplet state to be the lowest lying for all geometries, and for Pd₃₈ a s.m. of 9 is found. This is consistent with the increased number and decreased energetic spacing of the metal electronic states as the cluster size is increased.

A linear correlation between CO bondlength and vibrational frequency was observed for all cluster sizes (**Fig. 3a**). For any adsorbed state, r_{C-O} was longer and the stretching frequency lower than in the gas phase, evidencing adsorption-induced weakening of the CO bond in accordance with the Blyholder model [77]. This trend also seems insensitive to the choice of functional, since B3LYP and PBE data follow the same trendline. Similar correlations have been reported for Rh₄(3,1) clusters using smaller atom-centred basis sets (*i.e.* LanL2dz) [18], and a similar decrease in ν_{CO} observed via Infrared multiple photon dissociation (IR-MPD) spectroscopy for neutral Pd_nCO clusters where n = 6, 7, 8 and 9 [78]. It is evident from **Fig. 3b** that the CO bond weakens (ν_{C-O}) as the metal-carbonyl bond strength (ΔE_{ads}), increases, again consistent with the Blyholder model. The IR intensities of various adsorbed configurations roughly scaled in the same fashion for lCO, bCO and hCO species on Pd₄(3,1) and Pd₁₃(O_h), with lCO:bCO:hCO = 1.00:0.68:0.58 (**Fig. 4**). This intensity ratio was therefore employed to estimate relative band intensities during the IR simulations described later. In summary, the vibrational frequencies (ν_{C-O}) and intensities (I_{C-O}) of adsorbed CO are inversely proportional to the exothermicity of adsorption.

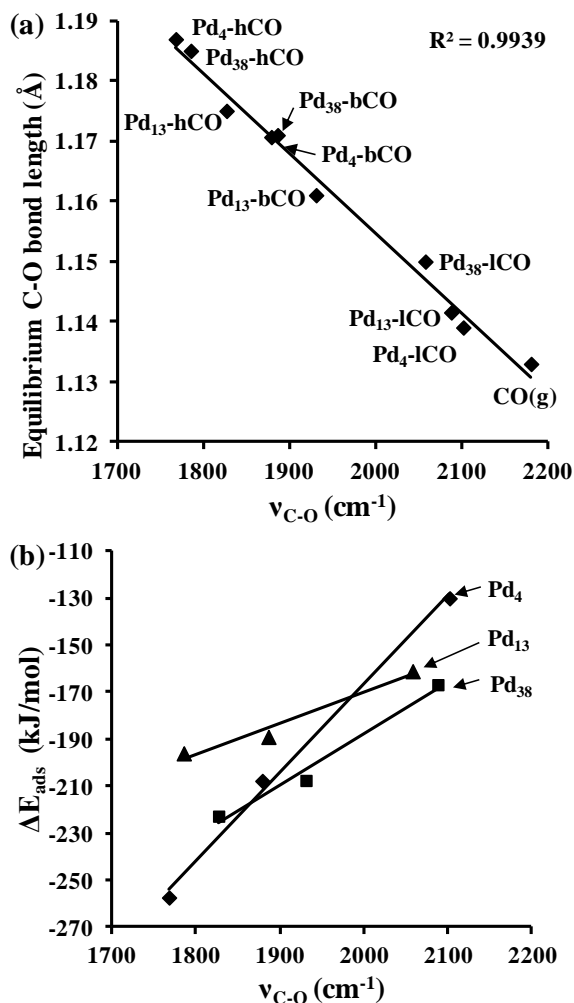


Figure 3. Correlation between (a) equilibrium C-O bondlength and CO vibrational frequency, and (b) CO adsorption energy and CO vibrational frequency, for a CO molecule on Pd₄, Pd₁₃ (B3LYP/CEP-121G(Pd),aug-cc-pVTZ(C,O)) and Pd₃₈ (PBE, planewaves, $E_{cut} = 500$ eV, 30Å cubic box) NPs.

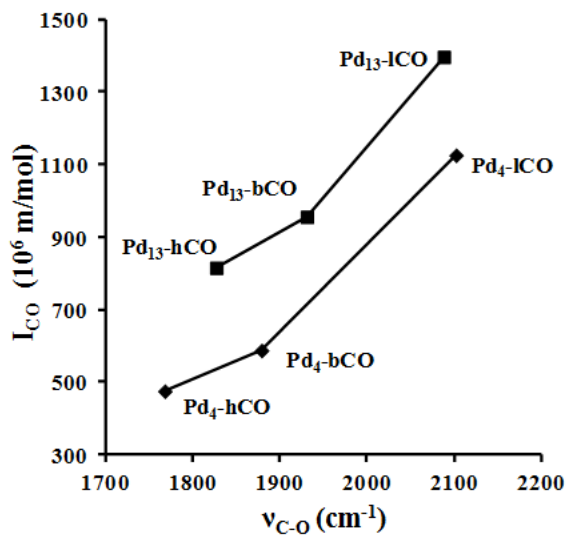


Figure 4. Correlation between the IR absorption intensity and CO vibrational frequency (B3LYP/CEP-121G(Pd),aug-cc-pVTZ(C,O)) for a CO molecule on Pd₄ and Pd₁₃ NPs.

3.2. Low coverage CO adsorption on Pd₃₈. In order to further explore the adsorption energetics of CO as $\theta_{\text{CO}} \rightarrow 0$, additional calculations were undertaken for CO placed at every symmetry unique linear, bridge and hollow position on the cubooctahedral Pd₃₈ NP (**Fig. 5**), using the PBE functional. Full optimisation of the NP/adsorbate system showed that certain adsorbed configurations were unstable (e.g. **bCO2**, **bCO4**), with the CO molecule relaxing into adjacent adsorption sites.

As expected, for the PBE functional, we find that linearly adsorbed CO has a lower adsorption energy on Pd₃₈ than bridge/hollow-bound CO. The weakest bound CO species on Pd₃₈ corresponded to linearly adsorbed CO at the vertex of the (100)-facet (**ICO1 = ICO₍₁₀₀₎**), followed by linearly adsorbed CO on a (111)-facet (**ICO2 = ICO₍₁₁₁₎**), with four-fold hollow-bound CO at the (100)-site (**hCO4 = hCO₍₁₀₀₎**) exhibiting a moderate adsorption strength. Bridge- (**bCO1 = bCO_(100/111)**) and hollow-bound CO (**hCO1 = hCO_(100/111)**) at the edge of the (100)/(111) facet were the next most stable configurations. The strongest adsorption site for CO at $\theta_{\text{CO}} \rightarrow 0$ was the 3f hollow bound CO (i.e. **hCO2**, **hCO3 = hCO_(111/111)**) to the (111)-like facets, or at the bridge site between two (111)-facets (**bCO3 = bCO_(111/111)**). Bridge-bound CO between two (111)-facets has been previously described as the most stable adsorption configuration for CO on alumina-supported Pd NPs [23]. Our calculations suggest that the 3f hollow bound CO (i.e. **hCO₍₁₁₁₎**) is practically isoenergetic with this for $\theta_{\text{CO}} \rightarrow 0$, in keeping with the previously reported weak facet specificity for CO adsorption in the low coverage limit [31]. In the following section we briefly evaluate the interaction of two hCO molecules on the Pd₃₈ surface before considering adsorption energetics at higher CO coverages.

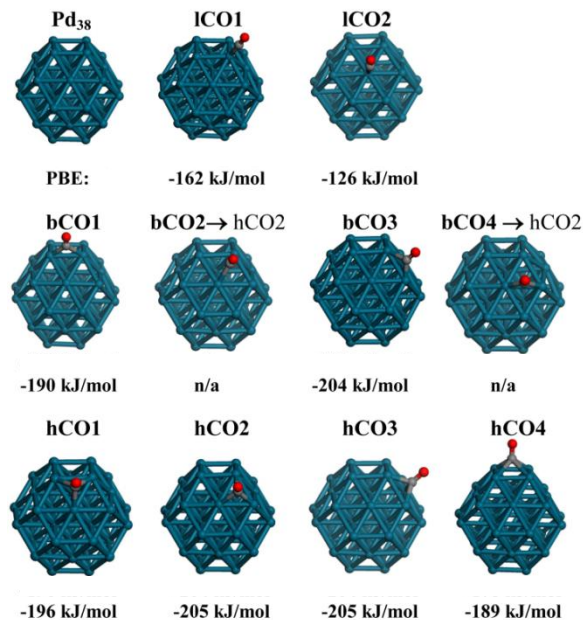


Figure 5. Symmetry unique adsorption sites and energies for Pd₃₈CO using the PBE XC functional.

3.3. High coverage CO adsorption on Pd₃₈. The influence of lateral interactions and charge sharing upon CO binding to a Pd₃₈ NP was studied by progressively increasing the number of co-adsorbed molecules. Structures in which two CO molecules were co-adsorbed at 3f hollow sites on Pd₃₈ were probed first, and a selection of these configurations are presented in **Fig. 6**. The most favourable scenario for this system is that in which both CO molecules share one Pd atom (i.e. **2hCO1**), however sharing of a second Pd atom (e.g. **2hCO2**) destabilised adsorption by $\sim 18 \text{ kJ}\cdot\text{mol}^{-1}$. The absence of any shared Pd atoms (e.g. **2hCO3**) is likewise disfavoured (by $11 \text{ kJ}\cdot\text{mol}^{-1}$) compared to that wherein a single surface Pd atom is shared.

A similar phenomenon is observed for four co-adsorbed CO molecules, for which the most stable structures are those in which all CO molecules share a single Pd atom, resulting in a ring of CO molecules around the (100) facet (**4COh4b0l0** in **Fig. 6**). The diffusion barrier of CO on Pd(110) surfaces determined by inelastic tunneling microscopy is $17.4 \text{ kJ}\cdot\text{mol}^{-1}$ [79]. At high coverages, this barrier is expected to fall, according to time-elapsd STM diffusivity studies of CO on Cu(111) which showed a doubling in the hopping rate with increasing local CO coverage [80]. Based on our static results above, and assuming fast CO diffusion kinetics on the NP surface, one would expect that all 3f hollow sites surrounding the six 4f hollow sites of Pd₃₈ would be occupied first as the CO coverage is further increased. We used this concept to create one set of models for predominantly hollow-bound Pd₃₈(CO)_n through *algorithm 1*. Specifically, *algorithm 1* involves: (a) occupy all 3f hollow sites around one of the six 4f hollows; then (b) add CO molecules to 3f hollow positions around adjacent 4f hollows while maximising the number of single, shared, Pd atoms between any two adsorbates; and finally (c) perform a full optimisation without symmetry constraints to permit relaxation to other bound configurations. The resulting structures built implementing *algorithm 1* are presented in **Fig. 6**, (**20COh16b4l0**, **16COh16b0l0**, **12COh12b0l0**, **8COh8b0l0**, and **4COh4b0l0**),

their associated energetics plotted against cluster size in **Fig. 7**, and more detailed data provided in **Table 2**. This methodology suggested that, even at the highest coverages, only hollow and bridge sites were occupied in the optimised structures. Using just *algorithm 1*, linearly-bound CO would not be sampled, and hence a second approach was also used to produce alternative site occupancies.

The second algorithm adopts a different approach based around the ‘domino effect’, to model repulsive interactions between high coverages of adjacent, linearly adsorbed CO molecules, rationalised previously for a $\text{Rh}_4(3,1)$ cluster [16] and to simulate low coverage adsorption from a less dense gas phase. *Algorithm 2* proceeds as follows: (a) place CO molecules on atop positions with their molecular axes pointing towards the centre of mass of the NP; then (b) adjust bondlengths so that all Pd-C and C-O bonds lengths equal 2.050 and 1.115 Å respectively, to emulate chemisorption from a weakly bound state; and finally (c) perform a full optimisation without symmetry constraints to permit relaxation of linear CO to bridge and hollow sites. This algorithm was utilised to generate the structures $32\text{COh}_{10}\text{b}_7\text{l}_{15}$, $24\text{COh}_2\text{b}_9\text{l}_{13}$, $12\text{COh}_0\text{b}_0\text{l}_{12}$, $6\text{COh}_0\text{b}_0\text{l}_6$, $4\text{COh}_0\text{b}_0\text{l}_4$, $2\text{COh}_0\text{b}_0\text{l}_2$ and $\text{COh}_0\text{b}_0\text{l}_1$, which are also included in **Fig. 6** and **Fig. 7** with additional detail in **Table 2**.

Algorithm 1 was based on observations from low PBE-energy arrangements for two and four CO molecules, wherein all possible adsorption combinations could be easily tested. *Algorithm 2* affords an additional test that initially places all CO molecules in the least energetically favourable atop site, such that at low coverages, adsorbate-adsorbate repulsive interactions are weak and CO molecules are trapped in local minima that prevent their relaxation into lower energy bridge and hollow sites; at high coverages, strong repulsive interactions enable linearly-bound CO to overcome small barriers associated with their movement into bridge or hollow sites, producing configurations in which all three types of adsorption site are populated. Such local energy minima in the DFT calculations are more likely to correspond to the experimental situation, wherein an atop preference should be observed at low coverage.

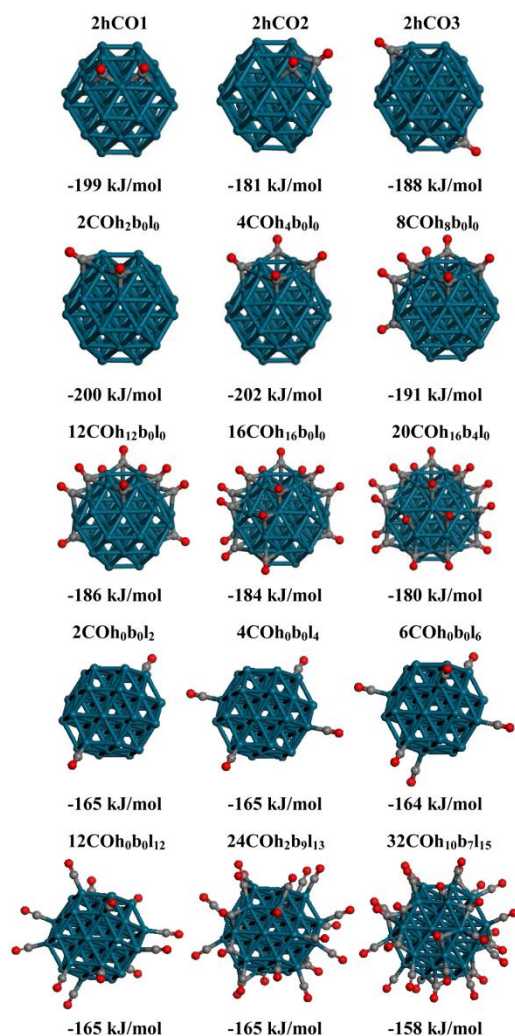


Figure 6. Structures and PBE adsorption energies per CO molecule of fully relaxed $\text{Pd}_{38}(\text{CO})_n$, where $n = 2, 4, 6, 8, 12, 16, 20, 24, 32$. Initial geometries obtained with coverage algorithms 1 and 2.

Fig. 7 shows that at low coverages *algorithm 2* yields much less favourable DFT adsorption energies than *algorithm 1*, since the former preserves as many as 12 linearly-bound CO molecules, whereas only hollow sites are occupied post-relaxation via the latter approach (see **Table 2**). We note that the adsorption energy per CO molecule weakens with increasing θ_{CO} for *algorithm 1*, but remains constant for *algorithm 2*. The coverage-dependent adsorption energy predicted by *algorithm 1* is in good agreement with microcalorimetric measurements of CO on supported model Pd NPs [31, 32, 81], which show a 20-40 kJ.mol⁻¹ decrease with θ_{CO} , and previous calculations on a Rh nanocluster which showed a 60 kJ.mol⁻¹ fall in the heat of CO adsorption with coverage [16]. Microcalorimetric measurements of the heats of CO adsorption on Pd/Al₂O₃, SiO₂ and TiO₂ having loadings of 2, 5 and 10 wt% Pd reported values spanning 99-162 kJ.mol⁻¹ [30], with high adsorption energies associated with low Pd loadings (i.e. smaller) and highly reduced particles. Our calculated, average CO adsorption energy of -159±1 kJ.mol⁻¹ on Pd₃₈ for $\theta = 1$ is in good agreement with the -162 kJ.mol⁻¹ measured by Dropsch and Baerns [30]. We have also explored two higher coverage regimes, Pd₃₈(CO)₃₈ ($\theta = 1.50$) and Pd₃₈(CO)₅₄ ($\theta = 1.69$), which yielded even lower heats of adsorption of -123.0 kJ.mol⁻¹ and -112.4 kJ.mol⁻¹ respectively.

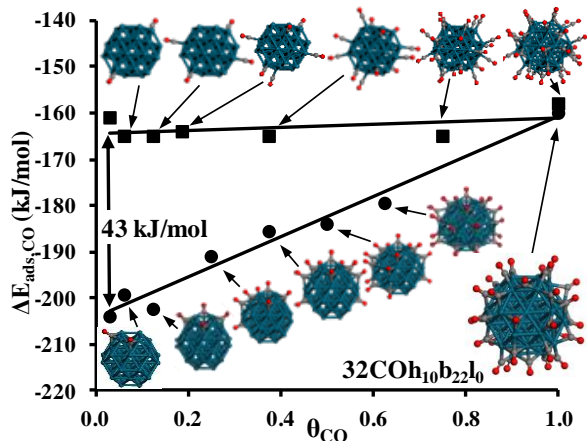


Figure 7. Coverage dependent CO adsorption energy ($\Delta E_{\text{ads,CO}}$, PBE) per molecule over cubooctahedral Pd₃₈ for structures obtained via (●) algorithm 1 and (■) algorithm 2, and for 32COh₁₀b₂₂l₀. Solid lines are least square fits to data points.

Table 2. Adsorption energy per CO on a Pd₃₈ NP as a function of CO coverage and adsorption site.

Label ^a	formula	θ_{CO}^b	$\Delta E_{\text{ads,CO}}^c$	n_{hCO}	n_{bCO}	n_{lCO}
32COh ₁₀ b ₂₂ l ₀	Pd ₃₈ (CO) ₃₂	1.000	-160	10	22	0
20COh ₁₆ b ₄ l ₀	Pd ₃₈ (CO) ₂₀	0.625	-180	16	4	0
16COh ₁₆ b ₀ l ₀	Pd ₃₈ (CO) ₁₆	0.500	-184	16	0	0
12COh ₁₂ b ₀ l ₀	Pd ₃₈ (CO) ₁₂	0.375	-186	12	0	0
8COh ₈ b ₀ l ₀	Pd ₃₈ (CO) ₈	0.250	-191	8	0	0
4COh ₄ b ₀ l ₀	Pd ₃₈ (CO) ₄	0.125	-202	4	0	0
2COh ₂ b ₀ l ₀	Pd ₃₈ (CO) ₂	0.063	-199	2	0	0
COh ₁ b ₀ l ₀	Pd ₃₈ (CO) ₁	0.031	-204	1	0	0
32COh ₁₀ b ₇ l ₁₅	Pd ₃₈ (CO) ₃₂	1.000	-158	10	7	15
24COh ₂ b ₉ l ₁₃	Pd ₃₈ (CO) ₂₄	0.750	-165	2	9	13
12COh ₀ b ₀ l ₁₂	Pd ₃₈ (CO) ₁₂	0.375	-165	0	0	12
6COh ₀ b ₀ l ₆	Pd ₃₈ (CO) ₆	0.188	-164	0	0	6
4COh ₀ b ₀ l ₄	Pd ₃₈ (CO) ₄	0.125	-165	0	0	4
2COh ₀ b ₀ l ₂	Pd ₃₈ (CO) ₂	0.063	-165	0	0	2
ICO1	Pd ₃₈ (CO) ₁	0.031	-161	0	0	1
	Pd ₃₈	0.000	-	-	-	-

^a Entries 2-8 and 9-15 have been calculated via algorithm 1 and 2, respectively.

^b CO surface coverage given by $n_{\text{CO}}/n_{\text{surf}}$, where $n_{\text{surf}} = 32$ for Pd₃₈

^c Adsorption energy change per CO in kJ/mol calculated using Eqn. 1

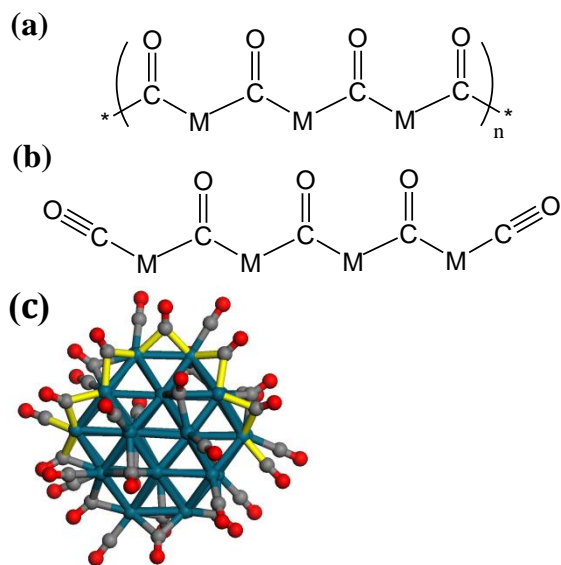
It is interesting to note that (at low coverages) CO bound in hollow sites is up to 43 kJ.mol⁻¹ more stable than that adsorbed in linear sites. However, this large energetic difference between linear and hollow bound CO vanishes at higher coverages (e.g. **20COh₁₆b₄l₀** and **24COh₂b₉l₁₃**). We have further tested this convergence by optimising a saturated CO monolayer structure (**32COh₁₀b₇l₁₅**, see **Table 3**). For this limiting coverage regime, the energy difference per CO molecule for different configurations (e.g. **32COh₁₀b₂₂l₀** versus **32COh₁₀b₇l₁₅**) falls below the threshold of thermal diffusion at STP (<2.5 kJ.mol⁻¹), suggesting that adsorption site populations will be fluxional as CO coverage nears saturation. Explicit calculation of the diffusion barrier at $\theta = 1$ was not possible due to the *coupled diffusion of CO molecules on Pd NP* at high coverages. For example, for **32COh₁₂b₇l₁₃**, the movement of one of the linearly-bound CO (lC₂₃O₁₀, see ESI for atom labels) to a nearby hollow-bound position causes the simultaneous relaxation of hC₇O₁₄ to bCO and lC₃₀O₃₁ to bCO. In another case (**32CO^hh₁₂b₇l₁₃**), movement of bC₂₂O₂₈ to a hollow site causes the simultaneous relaxation of lC₆O₁₃ and lC₁₈O₇ to hollows, and lC₁₃O₃ to a bridge site. In all cases examined, displacement of a single CO molecule triggered site-switching of multiple other co-adsorbates; the CO molecules so perturbed were not necessarily neighbouring the initially displaced CO molecule, but on occasion on the opposite side of the NP. Table 3 shows that the structures resulting from these displacements have close relative energies despite significant differences in their site populations. Experimental IR spectra of CO over Pd nanoparticles are measured almost exclusively at ‘high’ pressure/saturation θ_{CO} [15, 23, 82-84], hence it seems plausible that *algorithm 2*, which incorporates repulsive interactions between co-adsorbates and generates linear, bridge and hollow CO species, may be the most apposite among the 2 algorithms for simulating IR spectra of such Pd NP systems. Indeed, we later show that simulated IR absorption spectra using *algorithm 2* are in good agreement with experimental data for silica supported palladium NPs.

Table 3. Relative average CO adsorption energy as a function of adsorption site population at $\theta_{\text{CO}} = 1$

Label	$r\Delta E_{\text{ads}}^a$	n_{hCO}	n_{bCO}	n_{lCO}	action
32COh₁₀b₇l₁₅	0.0	10	7	15	original
32COh₁₂b₇l₁₃	0.1	12	7	13	lCO to hCO
32CO^hh₁₂b₇l₁₃	-1.0	12	7	13	bCO to hCO
32COh₁₁b₉l₁₂	-1.9	11	9	12	lCO to bCO
32COh₁₀b₂₂l₀	-2.3	10	22	0	all lCO to bCO

^a relative ΔE is difference between the ΔE per CO of 32lCO to that of Pd₃₈(CO)₃₂ where the number of each CO species was altered

Dropsch and Baerns also obtained coverage-dependent TPD-CO spectra that show a shift to lower temperature as a function of CO coverage, consistent with the falling heats of CO adsorption observe in **Fig. 7** [30]. At coverages <0.4 ML they only observed one CO desorption peak, while higher coverages resulted in three distinct adsorption states, consistent with the computed thermodynamic stability of hollow-bound CO at low coverage, and population of three bonding sites at $\theta_{\text{CO}} = 1$ as noted above. This TPD study also concluded that bridge-bound CO was the most abundant form over Pd NPs. From a thermodynamic viewpoint our calculations yield a similar conclusion, with the lowest energy structure for Pd₃₈(CO)₃₂ comprising mostly bridge-bound CO (i.e. **32COh₁₀b₂₂l₀**), and a minority hollow-bound. High CO coverages appear to energetically favour chains of bridged molecules, which may be closed, or as in this work, terminated by linear carbon monoxide (**Scheme 1**). Such chains of bridging CO molecules decorate the edges of the Pd₃₈(O_h) cubooctahedron, in line with high pressure (200 mbar) SFG studies which showed the existence of such CO species under catalytically relevant reaction conditions [23].



Scheme 1. Schematic of (a) closed and (b) open bridge-bound CO chains on a Pd₃₈ NP, and (c) three-dimensional ball and stick representation of Pd₃₈(CO)₃₂ showing open bridge CO chain in yellow.

It is conceivable that the motion in such CO chains is coupled, and indeed our subsequent vibrational analysis suggests that frequency-splitting occurs, demonstrating vibrational coupling of CO stretches; such splitting/shifting of CO vibrational bands has been previously reported on surfaces [85] and metal NPs [18]. Other thermodynamically stable structural motifs were also identified. For example, 1CO-hCO-1CO and even 1CO-hCO-1CO-hCO-1CO appeared in the optimised structures to have greater thermodynamic stability than isolated adsorbed CO configurations which one may have expected on the basis of reducing repulsive inter-adsorbate interactions.

3.4. IR simulations of Pd₃₈(CO)_n. At the PBE level, using a 30 Å cubic periodic box, the calculated vibrational frequency of gas phase CO is $\nu_{\text{CO,PBE}} = 2131 \text{ cm}^{-1}$ which is 49 cm^{-1} below the experimental value ($\nu_{\text{exp}} = 2180 \text{ cm}^{-1}$) [18]. We therefore add 49 cm^{-1} to the calculated vibrational frequencies for the PBE simulations using CO on the Pd₃₈ cluster to make easier comparison with experimental data. IR simulations based on these intensity estimates from B3LYP calculations of the smaller clusters were carried out using optimised structures from *algorithm 1* (20COh₁₆b₄l₀, 16COh₁₆b₀l₀, 12COh₁₂b₀l₀, 8COh₈b₀l₀, 4COh₄b₀l₀) and *algorithm 2* (32COh₁₀b₇l₁₅, 24COh₂b₉l₁₃, 12COh₀b₀l₁₂, 6COh₀b₀l₆, 4COh₀b₀l₄, 2COh₀b₀l₂, COh₀b₀l₁). Simulated spectra are shown in **Fig. 8a-b**, alongside a comparative experimental DRIFTS spectrum for CO adsorbed over a 2.22 wt% Pd/KIT-6 mesoporous catalyst, with mean Pd NP diameter of 1.7 nm (**Fig. 8c**).

IR spectra simulated via *algorithm 1* display significant vibrational coupling, evidenced by fine structure within the hollow-bound CO band, which (albeit infrequently present) appears as a weak, broad feature in DRIFT spectra of supported catalysts [18]. **Fig. 8a** also shows the presence of bridge-bound CO at intermediate coverages ($\theta_{\text{CO}} = 0.625$), which overlaps with hollow CO features, indicative of similar adsorption energetics at high coverage. The latter observation is consistent with the weakening Pd-hCO bond with increasing θ_{CO} from 0.03 \rightarrow 0.625 apparent in **Fig. 7**, which induces a pronounced 63 cm^{-1} blue-shift in the hCO band average position. A similar, albeit, weaker blue-shift (29 cm^{-1} , **Fig. 8b**) was observed with increasing θ_{CO} for linearly-bound CO bands simulated via *algorithm 2*.

The utility of these simulations was assessed for Pd₃₈(CO)₃₂ by benchmarking against frequency ranges and band assignment for RAIRS studies on model Pd/Al₂O₃ catalysts [86] and vibrational sum frequency generation (SFG) of CO adsorption on Pd NPs and Pd(111) surfaces [39]. The RAIRS study of Wolter et al recorded absorption spectra for CO on nanoparticles ranging from Pd_{<10} to Pd₇₁₀₀ at 90 and 300 K. Features between 1930-2000 cm^{-1} were assigned to bridge-bound CO, and those between 2090-2120 cm^{-1} to linearly-bound CO. These compare extremely favourably to corresponding predictions of 1920-1983 cm^{-1} and 2062-2106 cm^{-1} from our simulations using *algorithm 2* (**Fig. 8b**). The signal from hollow CO (hCO) was reported to be weak in these RAIRS experiments, however photoelectron diffraction studies [27] and RAIRS measurements over Pd(111) at temperatures $<200 \text{ K}$ and $>350 \text{ K}$ [87] suggest an indicative stretching frequency between 1825-1900 cm^{-1} (cf. 1843-1898 cm^{-1} in **Fig. 8c**). Agreement between the present calculations at $\theta_{\text{CO}} = 1$ via *algorithm 2* and experimental observations is astonishingly good. Band positions and relative intensities of linear and bridge-bound CO from our simulations are also in excellent correspondence with the DRIFT spectrum of a saturated CO adlayer over a 2.22 wt% Pd/KIT-6 catalyst [15] (**Fig. 8c**). The extremely weak experimental hCO band for Pd NPs supported on the KIT-6 mesoporous silica likely reflects a combination of (i) the smaller IR absorption coefficients with respect to bCO and lCO (**Fig. 4**), and (ii) the experimental protocol, in which the Pd catalyst was flushed with an inert gas after CO adsorption at 298

K prior to spectral acquisition [15]; thermodynamics suggest that CO is only stable in hollow sites at ambient temperature under CO partial pressures exceeding 1000 mbar [87].

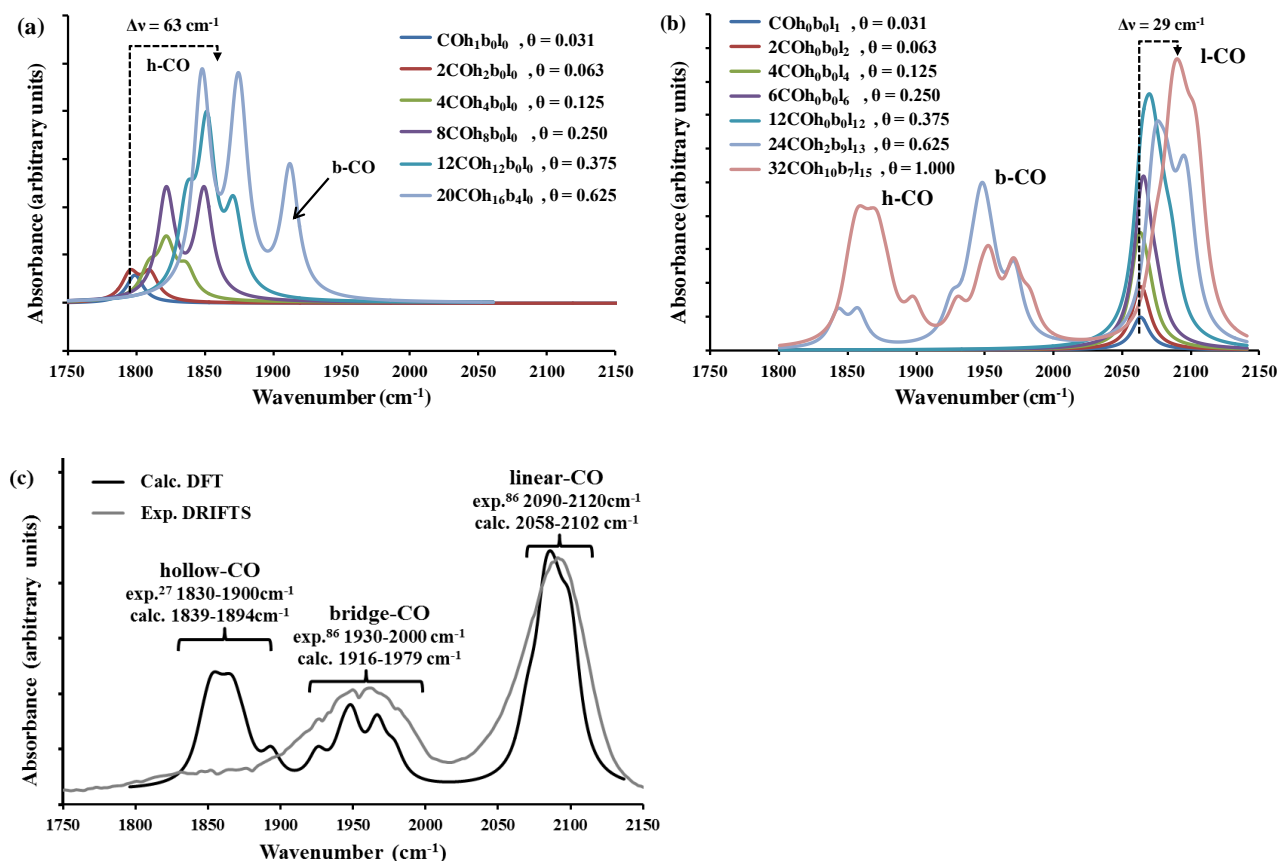


Figure 8. Simulated IR absorption spectra for a range of $\text{Pd}_{38}(\text{CO})_n$ structures created with (a) *algorithm 1*, (b) *algorithm 2* and (c) comparison of *algorithm 2* with experimental DRIFTS spectrum of CO on Pd/KIT-6 for $\theta_{\text{CO}} = 1$. Oscillator intensities scaled in the ratio $\text{ICO}:\text{bCO}:\text{hCO} = 1.00:0.68:0.58$ taken from Pd_{13} in **Fig. 4**. Frequencies have been shifted by 49 cm^{-1} which is the difference between the calculated vibrational frequency of gas phase CO ($\nu_{\text{CO,PBE}} = 2131 \text{ cm}^{-1}$) and the experimental value ($\nu_{\text{exp}} = 2180 \text{ cm}^{-1}$) [18].

3.5. Coverage-dependent blue-shift of CO on Pd_{38} . The preceding coverage-dependent vibrational frequencies for CO in each of the three adsorption sites over a $\text{Pd}_{38}(\text{O}_h)$ NP derived via *algorithms 1* and *2* are summarised in **Fig. 9**. In all cases, the CO stretch exhibited a significant blue-shift with increasing coverage, with the sensitivity of this shift in the order $\text{hCO} > \text{bCO} > \text{ICO}$, akin to that observed in electrochemical RAIRS studies of CO adlayers on Pd(110), which demonstrated a 10 cm^{-1} blue-shift for $\theta_{\text{CO}} = 0 \rightarrow 1$ [88]. We attribute the stronger coverage-dependence observed herein to quantum size effects, and note that an earlier study of CO adsorption on $\text{Rh}_4(3,1)$ reported an even greater blue-shift of 80 cm^{-1} [16]. The coverage-dependent blue-shift may therefore provide a means by which to differentiate between hollow and bridge/linear bound CO in experimental IR spectroscopy. This consistent blue-shift for all adsorption configurations indicates strengthening of the C-O bond, and concurrent weakening of the M-CO bond. Based on the Blyholder [77] and Bagus [89] interpretations of the metal-carbonyl bond, this weakening reflects reduced electron donation from occupied d-states on the metal into the doubly degenerate, anti-bonding $2\pi^*$ molecular orbital of CO, increasing the covalency of the C=O bond and hence force constant.

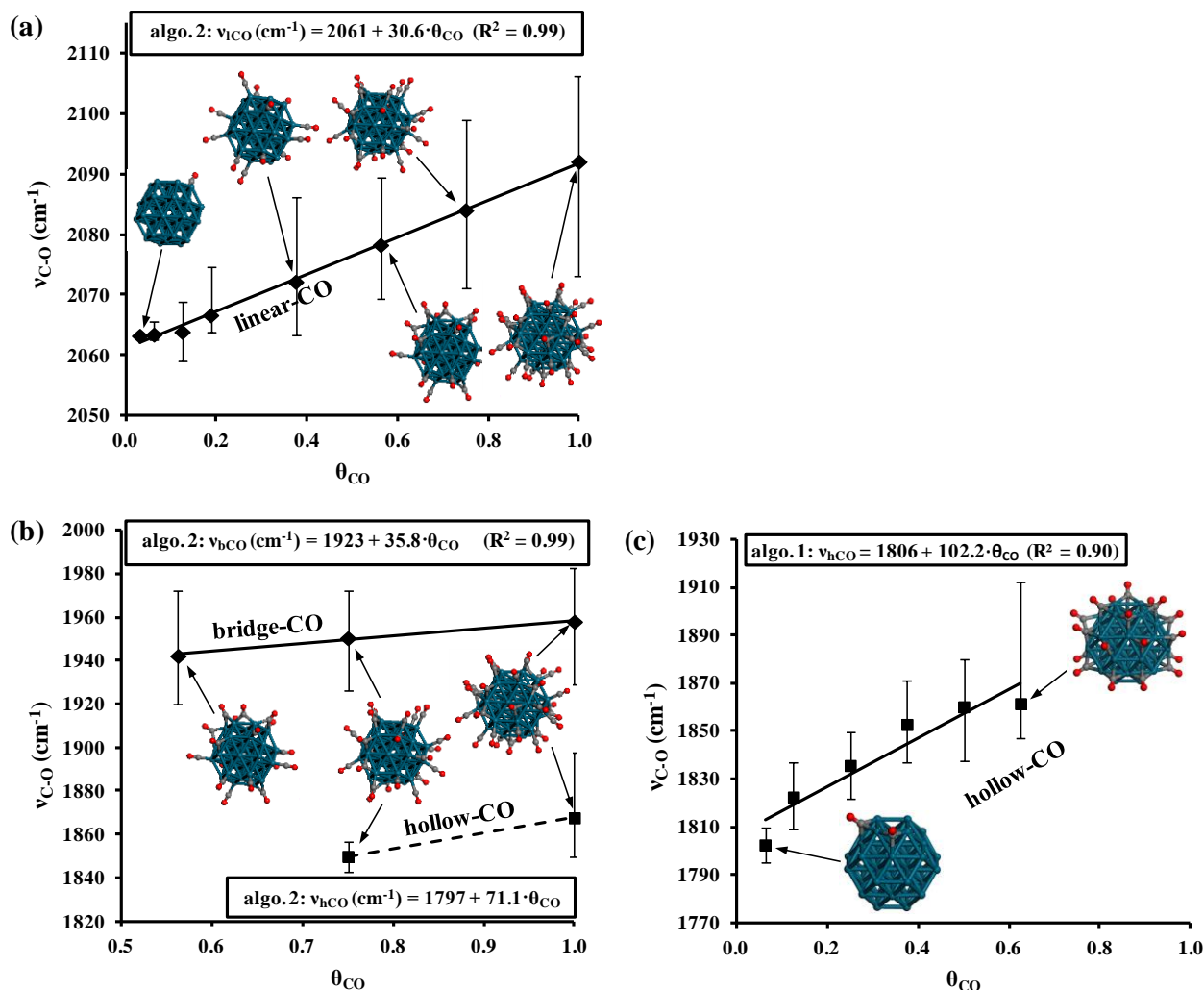


Figure 9. Mean CO vibrational stretching frequency of (a) linear and (b) bridge (—) and hollow (---) bound CO from *algorithm 2*, and (c) hollow bound CO from *algorithm 1*, as a function of θ_{CO} on a Pd_{38} NP. Error bars show the maximum/minimum values.

3.6. Coverage-dependent isotropic expansion of Pd_{38} . Adsorbate-induced lattice expansion is well known for extended surfaces and NPs through diffraction studies [90], and has been demonstrated computationally for hydrogen on Pd_6 and Pd_{13} NPs [91]. In view of the above variation in CO adsorption strength with coverage, we therefore computed the mean Pd-Pd bondlength ($r_{\langle \text{Pd-Pd} \rangle}$) and accompanying variance ($\sigma_{\langle \text{Pd-Pd} \rangle}$) in order to identify whether a similar lattice expansion occurs in the $\text{Pd}_{38}(\text{CO})_n$ system. Results of this analysis are shown in **Fig. 10** for structures obtained via *algorithms 1* and 2. The average Pd-Pd bondlength of the Pd_{38} NP increased by $>3.5\%$ as $\theta_{CO} = 0 \rightarrow 1$, a striking lattice expansion that was approximately proportional to the number of adsorbed CO molecules. The origin of this expansion lies in the overall increase in charge transfer from the Pd_{38} NP into adsorbate bonds with increasing CO coverage, and hence weaker cohesive metallic bonding. It is important to note that while the adsorption energy per CO molecule falls with θ_{CO} from approximately $-200 \text{ kJ}\cdot\text{mol}^{-1}$ over the bare particle to $-160 \text{ kJ}\cdot\text{mol}^{-1}$ at saturation, this is more than compensated for by the increasing number of Pd-CO bonds formed, and hence rise in total adsorption energy and consequent perturbation of the intraparticle bonding. Structures derived by *algorithm 1* always exhibited larger expansions than those derived by *algorithm 2*, although the associated spread of bondlengths $\sigma_{\langle \text{Pd-Pd} \rangle}$ was also greater. Both these observations are consistent with stronger bonding of hollow versus linearly-bound CO, and hence larger perturbation of the underlying Pd_{38} NP framework. *Algorithms 1* and 2 predict significantly different sensitivities of $r_{\langle \text{Pd-Pd} \rangle}$ to θ_{CO} , providing an avenue for experimentally testing whether CO adsorption commences via all hollow (*algorithm 1*) or mixed adsorption (*algorithm 2*) structures via e.g. coverage dependent EXAFS, one of the few techniques able to precisely measure interatomic distances of sub-2 nm NPs under reactive environments. This observation may also explain the low population of the hollow site usually seen experimentally (e.g. in the DRIFTS spectrum of **Fig. 8**). The Pd_{38} cluster used in our calculations is at the smaller length scale of those generally

prepared experimentally, and likely exhibits greater surface flexibility than larger clusters, more readily accommodating the Pd-Pd bond expansion required for hollow site occupation.

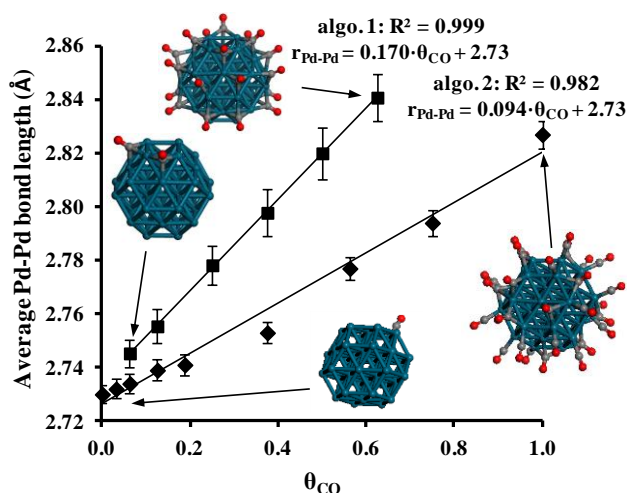


Figure 10. Mean Pd-Pd bondlength of Pd₃₈ NP as a function of CO coverage. Error bars show the standard deviation.

The narrow distribution of Pd-Pd bondlengths observed for each CO coverage, evidenced by the small values of $\sigma_{\langle \text{Pd-Pd} \rangle}$ in **Fig. 10**, strongly indicates that the Pd₃₈ NP lattice expansion is isotropic. From a catalytic perspective, the implication is that variations in surface CO coverage under reaction conditions could systematically regulate isotropic expansion/contraction of palladium NPs, and hence influence molecular co-adsorption, bond activation and ultimately both activity and selectivity (as is reported for O and CO adsorption and CO dissociation over Ru(0001) [92] wherein DFT calculations of Mavrikakis et al demonstrate an increase in surface reactivity with lattice expansion). Coverage-dependent CO DRIFTS studies would offer another means to experimentally verify our predicted lattice expansion of palladium nanoparticles, since **Fig. 8** suggests this occurs concomitant with a 63 and 29 cm⁻¹ blue-shift in the respective hCO and lCO bands, with the latter a strong feature of experimental CO absorption spectra.

CONCLUSIONS

B3LYP and PBE DFT calculations have been combined to obtain information on IR spectroscopic adsorption frequencies and intensities for CO chemisorption over Pd nanoparticles as a function of particle size (i.e. Pd₄, Pd₁₃ and Pd₃₈) and CO coverage. IR absorption spectra were subsequently simulated for a Pd₃₈ nanoparticle, employing two computational approaches to obtain optimised Pd₃₈CO_n structures. Calculated IR spectra using the B3LYP XC-functional to estimate the IR intensities, and PBE to give estimated frequencies, are in good agreement with experimental DRIFTS spectrum for CO adsorption over 2.22% Pd nanoparticles supported on a KIT-6 silica [15] provided a mixed population of hollow, bridge and atop species are included, and RAIRS and SFG studies of model Pd nanoparticle catalysts [39, 86]. At low coverages ($\theta \rightarrow 0$) we find adsorption energy trends in good agreement with earlier work, and show that the dependence on particle size depends on adsorption site, with hollow and bridge sites showing adsorption energies that are more favourable on small clusters, and linear sites showing a weakening in adsorption as cluster size decreases. At high CO coverages ($\theta = 1$) linearly, bridge- and hollow-bound CO co-exist, with very small energy differences between alternative arrangements of CO molecules at different adsorption sites. Diffusion between sites is then thermally feasible at STP via a coupled diffusion process, and the equilibrium arrangement may be influenced by the additional entropy of occupying different sites. Elevated coverages of CO favour the formation of bridge-bound CO chains over a Pd₃₈ nanoparticle, with some hollow-bound CO. A coverage-dependent spectroscopic blue-shift is predicted in the vibrational IR bands of adsorbed CO, coincident with an isotropic 3.5 % expansion of the palladium nanoparticle framework, which could a factor in driving adsorption-induced enhancements in catalytic activity for reactions involving CO.

AUTHOR INFORMATION

Corresponding Authors

*Constantinos D. Zeinalipour-Yazdi, E-mail: c.zeinalipour-yazdi@ucl.ac.uk; David J. Willock, E-mail: WillockDJ@cardiff.ac.uk; and Adam F. Lee, E-mail: A.F.Lee@aston.ac.uk

Author Contributions

The manuscript was written through contributions of all authors.

Funding Sources

We thank the EPSRC (EP/E046754/1; EP/G007594) for financial support and the award of a leadership fellowship (AFL).

ACKNOWLEDGMENT

This work used the ARCHER UK National Supercomputing Service (<http://www.archer.ac.uk>), Wales' national supercomputing service provider, High Performance Computing (HPC) Wales, and the ARCCA HPC Cluster (Raven). Dr. Christopher Parlett (Aston University) is thanked for providing a DRIFT spectrum of CO adsorbed over a 2.22% Pd/KIT-6 catalyst.

SUPPORTING INFORMATION

The relative energy of Pd₄(3,1) using various XC-functionals (**S-Fig. 1**) and the adsorption energies and vibrational frequencies for CO on Pd₃₈ using PBE and B3LYP (**S-Table 1**) as well as the Cartesian coordinates (**S-Table 2**) of all optimized models are provided as supporting information. The correlation of Pd₃₈ NP isotropic expansion with CO vibrational frequency is shown in **S-Fig. 2**.

ABBREVIATIONS

IR, infrared; UHV, ultra-high vacuum; DFT, density functional theory; DRIFTS, Diffuse reflectance infrared Fourier-transform spectroscopy; TPD, temperature-programmed desorption; MCSCF, multi-configurational self-consistent-field; RAIRS, reflection absorption infrared spectroscopy; SCE, Saturated calomel electrode; SFG, sum-frequency generation; IR-MPD; Infrared multiple photon dissociation.

REFERENCES

- [1] M.S. Chen, Y. Cal, Z. Yan, K.K. Gath, S. Axnanda, D.W. Goodman, Highly active surfaces for CO oxidation on rh, pd, and pt, *Surf. Sci.*, 601 (2007) 5326-5331.
- [2] A. Haynes, Chapter 1 - Catalytic Methanol Carbonylation, in: C.G. Bruce, K. Helmut (Eds.) *Advances in Catalysis*, Academic Press, 2010, pp. 1-45.
- [3] R. Franke, D. Selent, A. Börner, *Applied Hydroformylation*, *Chemical Reviews*, 112 (2012) 5675-5732.
- [4] R.J. Behm, K. Christmann, G. Ertl, M.A. Van Hove, Adsorption of CO on Pd(100), *J. Chem. Phys.*, 73 (1980) 2984-2995.
- [5] P.J. Berlowitz, C.H.F. Peden, D.W. Goodman, Kinetics of Carbon Monoxide Oxidation on Single-Crystal Palladium, Platinum, and Iridium, *J. Phys. Chem.*, 92 (1988) 5213-5221.
- [6] T. Engel, G. Ertl, A Molecular Beam Investigation of the Catalytic Oxidation of CO on Pd (111) *J. Chem. Phys.*, 69 (1978) 1267.
- [7] T. Engel, G. Ertl, Elementary Steps in the Catalytic Oxidation of Carbon Monoxide on Platinum Metals, *Adv. Catal.*, 28 (1979) 1-78.
- [8] A. Logan, M.T. Paffett, Steady-State co Oxidation Kinetics Over the Pd(100) Single Crystal Surface and the c(2 × 2)-Sn/Pd(100) Bimetallic Surface Alloy, *J. Catal.*, 133 (1992) 179-190.
- [9] H.S. Gandhi, G.W. Graham, R.W. McCabe, Automotive Exhaust Catalysis, *J. Catal.*, 216 (2003) 433-442.
- [10] C.D. Zeinalipour-Yazdi, A.M. Efstathiou, Preadsorbed Water-Promoted Mechanism of the Water-Gas Shift Reaction, *J. Phys. Chem. C*, 112 (2008) 19030-19039.
- [11] N.P. Lebedeva, M.T.M. Koper, E. Herrero, J.M. Feliu, R.A. van Santen, CO oxidation on stepped Pt[n(111) x (111)] electrodes, *J. Electroanal. Chem.*, 487 (2000) 37-44.
- [12] A.C. Lausche, A.J. Medford, T.S. Khan, Y. Xu, T. Bligaard, F. Abild-Pedersen, J.K. Nørskov, F. Studt, On the effect of coverage-dependent adsorbate-adsorbate interactions for CO methanation on transition metal surfaces, *J. Catal.*, 307 (2013) 275-282.
- [13] S. Shan, V. Petkov, L. Yang, J. Luo, P. Joseph, D. Mayzel, B. Prasai, L. Wang, M. Engelhard, C.J. Zhong, Atomic-structural synergy for catalytic CO oxidation over palladium-nickel nanoalloys, *Journal of the American Chemical Society*, 136 (2014) 7140-7151.
- [14] A.F. Lee, C.V. Ellis, K. Wilson, N.S. Hondow, In situ studies of titania-supported Au shell-Pd core nanoparticles for the selective aerobic oxidation of crotyl alcohol, *Catal. Today*, 157 (2010) 243-249.
- [15] C.M.A. Parlett, D.W. Bruce, N.S. Hondow, M.A. Newton, A.F. Lee, K. Wilson, Mesoporous Silicas as Versatile Supports to Tune the Palladium-Catalyzed Selective Aerobic Oxidation of Allylic Alcohols, *ChemCatChem*, 5 (2013) 939-950.
- [16] C.D. Zeinalipour-Yazdi, R.A. van Santen, Coverage-Dependent Adsorption Energy Trends of CO on a Rhodium Nanocluster, *J. Phys. Chem. C*, 116 (2012) 8721-8730.
- [17] C.D. Zeinalipour-Yazdi, A.L. Cooksy, A.M. Efstathiou, CO Adsorption on Transition Metal Clusters: Trends from Density Functional Theory, *Surf. Sci.*, 602 (2008) 1858-1862.

- [18] C.D. Zeinalipour-Yazdi, A.L. Cooksy, A.M. Efstathiou, A Diffuse Reflectance Infrared Fourier-Transform Spectra and Density Functional Theory Study of CO Adsorption on Rh/ γ -Al₂O₃, *J. Phys. Chem. C*, 111 (2007) 13872-13878.
- [19] K.A. Kacprzak, I. Czekaj, J. Mantzaras, DFT Studies of Oxidation Routes for Pd₉ Clusters Supported on γ -Alumina, *Phys. Chem. Chem. Phys.*, 14 (2012) 10243-10247.
- [20] Z.-P. Liu, S.J. Jenkins, D.A. King, Origin and Activity of Oxidized Gold in Water-Gas-Shift Catalysis, *Phys. Rev. Lett.*, 94 (2005) 196102.
- [21] L.M. Molina, B. Hammer, Theoretical study of CO oxidation on Au nanoparticles supported by MgO(100)..., *Phys. Rev. B*, 69 (2004) 155424.
- [22] D.A.J.M. Ligthart, R.A. van Santen, E.J.M. Hensen, Supported rhodium oxide nanoparticles as highly active CO oxidation catalysts, *Ang. Chem. - Int. Ed.*, 50 (2011) 5306-5310.
- [23] I.V. Yudanov, R. Sahnoun, K.M. Neyman, N. Rösch, J. Hoffmann, S. Schaueremann, V. Johánek, H. Unterhalt, G. Rupprechter, J. Libuda, H.-J. Freund, CO Adsorption on Pd Nanoparticles: Density Functional and Vibrational Spectroscopy Studies, *J. Phys. Chem. B*, 107 (2003) 255-264.
- [24] H. Unterhalt, G. Rupprechter, H.-J. Freund, Vibrational Sum Frequency Spectroscopy on Pd(111) and Supported Pd Nanoparticles: CO Adsorption from Ultrahigh Vacuum to Atmospheric Pressure, *J. Phys. Chem. B*, 106 (6) 356-367.
- [25] G. Rupprechter, H. Unterhalt, M. Morkel, P. Galletto, L. Hu, H.-J. Freund, Sum Frequency Generation Vibrational Spectroscopy at Solid-Gas Interfaces: CO Adsorption on Pd Model Catalysts at Ambient Pressure, *Surf. Sci.*, 502-503 (2002) 109-122.
- [26] T. Dellwig, G. Rupprechter, H. Unterhalt, H.-J. Freund, Bridging the Pressure and Materials Gaps: High Pressure Sum Frequency Generation Study on Supported Pd Nanoparticles, *Phys. Rev. Lett.*, 85 (2000) 776.
- [27] V. Fernandez, T. Giessel, O. Schaff, K.M. Schindler, A. Theobald, C.J. Hirschmugl, S. Bao, A.M. Bradshaw, C. Baddeley, A.F. Lee, R.M. Lambert, D.P. Woodruff, V. Fritzsche, A photoelectron diffraction study of the Pd{111}(root 3x root 3)R30 degrees-CO chemisorption phase, *Z. Phys. Chemie-Int. J. Res. Phys. Chem. Chem. Phys.*, 198 (1997) 73-85.
- [28] M. Tüshaus, W. Berndt, H. Conrad, A.M. Bradshaw, B. Persson, Understanding the structure of high coverage CO adlayers, *Appl. Phys. A*, 51 (1990) 91-98.
- [29] J. Szanyi, D.W. Goodman, CO Oxidation on Palladium. I. A Combined Kinetic-Infrared Reflection Absorption Spectroscopic Study of Pd(100), *J. Phys. Chem.*, 98 (1994) 2972-2977.
- [30] H. Dropsch, M. Baerns, CO Adsorption on Supported Pd Catalysts Studied by Adsorption Microcalorimetry and TPD, *Appl. Catal. A: Gen.*, 158 (1997) 163-183.
- [31] J.M. Flores-Camacho, J.-H. Fischer-Wolfarth, M. Peter, C.T. Campbell, S. Shaueremann, H.-J. Freund, Adsorption Energetics of CO on Supported Pd Nanoparticles as a Function of Particle size by Single Crystal Microcalorimetry, *Phys. Chem. Chem. Phys.*, 13 (2011) 16800-16810.
- [32] J.-H. Fischer-Wolfarth, J.A. Farmer, J.M. Flores-Camacho, A. Genest, I.V. Yudanov, N. Rösch, C.T. Campbell, S. Schaueremann, H.-J. Freund, Particle-size dependent heats of adsorption of CO on supported Pd nanoparticles as measured with a single-crystal microcalorimeter, *Phys. Rev. B*, 81 (2010).
- [33] P.J. Feibelman, B. Hammer, J.K. Nørskov, F. Wagner, M. Scheffler, R. Stumpf, R. Watwe, J. Dumesic, The CO/Pt(111) Puzzle, *J. Phys. Chem. B*, 105 (2001) 4018.
- [34] B. Hammer, Y. Morikawa, J.K. Nørskov, CO Chemisorption at Metal Surfaces and Overlayers, *Physical Review Letters*, 76 (1996) 2141-2144.
- [35] V. Bertin, E. Agacino, R. López-Rendon, E. Poulain, The CO Chemisorption on Some Active Sites of Pd Clusters: A DFT Study, *J. Molec. Struct.: THEOCHEM*, 796 (2006) 243-248.
- [36] P. Sautet, M.K. Rose, J.C. Dunphy, S. Behler, M. Salmeron, Adsorption and energetics of isolated CO molecules on Pd(111), *Surface Science*, 453 (2000) 25-31.
- [37] J.A. Herron, S. Tonelli, M. Mavrikakis, Atomic and molecular adsorption on Pd(111), *Surface Science*, 606 (2012) 1670-1679.
- [38] M.K. Rose, T. Mitsui, J. Dunphy, A. Borg, D.F. Ogletree, M. Salmeron, P. Sautet, Ordered structures of CO on Pd(111) studied by STM, *Surface Science*, 512 (2002) 48-60.
- [39] M. Morkel, H. Unterhalt, T. Klüner, G. Rupprechter, H.-J. Freund, Interpreting Intensities in Vibrational Sum Frequency Generation (SFG) Spectroscopy: CO Adsorption on Pd Surfaces, *Surf. Sci.*, 586 (2005) 146-156.
- [40] I.V. Yudanov, M. Metzner, A. Genest, N. Rösch, Size-Dependence of Adsorption Properties of Metal Nanoparticles: a DFT study on Palladium Nanoclusters, *J. Phys. Chem. C*, 112 (2008) 20269-20275.
- [41] I.V. Yudanov, A. Genest, S. Schaueremann, H.-J. Freund, N. Rösch, Size Dependence of the Adsorption Energy of CO on Metal Nanoparticles: a DFT Search for the Minimum Value, *Nano letters*, 12 (2012) 2134-2139.
- [42] B. Zhu, G. Thrimurthulu, L. Delannoy, C. Louis, C. Mottet, J. Creuze, B. Legrand, H. Guesmi, Evidence of Pd Segregation and Stabilization at Edges of AuPd Nano-Clusters in the Presence of CO: A Combined DFT and DRIFTS Study, *J. Catal.*, 308 (2013) 272-281.
- [43] R.C. Gaussian 09, M. J. Frisch, G. W. Trucks, H. B. Schlegel, G. E., M.A.R. Scuseria, J. R. Cheeseman, G. Scalmani, V. Barone, B. Mennucci,, M.C. G. A. Petersson, in, Gaussian Inc., Wallingford CT, 2009.

- [44] A.D. Becke, Density-Functional Thermochemistry. III. The Role of Exact Exchange, *J. Chem. Phys.*, 98 (1993) 5648.
- [45] C. Lee, W. Yang, R.G. Parr, Development of the Colle-Salvetti Correlation-Energy Formula into a Functional of the Electron Density, *Phys. Rev. B*, 37 (1988) 785.
- [46] Y. Zhao, D.G. Truhlar, The M06 Suite of Density Functionals for Main Group Thermochemistry, Thermochemical Kinetics, Noncovalent Interactions, Excited States, and Transition Elements: Two New Functionals and Systematic Testing of four M06-Class Functionals and 12 Other Functionals, *Theor. Chem. Acc.*, 120 (2008) 215-241.
- [47] J.M. Tao, J.P. Perdew, V.N. Staroverov, G.E. Scuseria, Climbing the Density Functional Ladder: Nonempirical Meta-Generalized Gradient Approximation Designed for Molecules and Solids, *Phys. Rev. Lett.*, 91 (2003) 146401.
- [48] O.A. Vydrov, G.E. Scuseria, J.P. Perdew, Tests of Functionals for Systems with Fractional Electron Number, *J. Chem. Phys.*, 126 (2007) 154109.
- [49] J.P. Perdew, K. Burke, M. Ernzerhof, Generalized Gradient Approximation Made Simple, *Phys. Rev. Lett.*, 77 (1996) 3865-3868.
- [50] C. Adamo, V. Barone, Exchange Functionals With Improved Long-Range Behavior and Adiabatic Connection Methods Without Adjustable Parameters: The mPW and mPW1PW Models, *J. Chem. Phys.*, 108 (1998) 664-675.
- [51] W.J. Hehre, R.F. Stewart, J.A. Pople, Self-Consistent Molecular Orbital Methods. 1. Use of Gaussian expansions of Slater-Type Atomic Orbitals, *J. Chem. Phys.*, 51 (1969) 2657-2664.
- [52] W.R. Wadt, P.J. Hay, Ab Initio Effective Core Potentials for Molecular Calculations - Potentials for Main Group Elements Na to Bi, *J. Chem. Phys.*, 82 (1985) 284-298.
- [53] T.H. Dunning Jr., P.J. Hay, *Modern Theoretical Chemistry*, Plenum, New York, 1976.
- [54] W.J. Stevens, H. Basch, M. Krauss, Compact Effective Potentials and Efficient Shared-Exponent Basis-Sets for the 1st-Row and 2nd-Row Atoms, *J. Chem. Phys.*, 81 (1984) 6026-6033.
- [55] W.J. Stevens, M. Krauss, H. Basch, P.G. Jasien, Relativistic Compact Effective Potentials and Efficient, Shared-Exponent Basis Sets for The Third-, Fourth-, and Fifth-Row Atoms, *Can. J. Chem.*, 70 (1992) 612-630.
- [56] D.E. Woon, T.H. Dunning Jr., Gaussian Basis Sets for Use in Correlated Molecular Calculations. III. The Atoms Aluminum Through Argon *J. Chem. Phys.*, 98 (1993) 1358.
- [57] A. Wilson, T. van Mourik, T.H. Dunning Jr., Gaussian Basis Sets for Use in Correlated Molecular Calculations. VI. Sextuple Zeta Correlation Consistent Basis Sets for Boron Through Neon, *J. Mol. Struct.*, 388 (1997) 339-349.
- [58] K.A. Peterson, D.E. Woon, T.H. Dunning Jr., Benchmark Calculations with Correlated Molecular Wave Functions. IV. The Classical Barrier Height of the $H+H_2 \rightarrow H_2+H$ Reaction, *J. Chem. Phys.*, 100 (1994) 7410.
- [59] R.A. Kendall, T.H. Dunning Jr., R.J. Harrison, Electron Affinities of the First-Row Atoms Revisited. Systematic Basis Sets and Wave Functions *J. Chem. Phys.*, 96 (1992) 6796.
- [60] T.H. Dunning Jr., Gaussian Basis Sets for use in Correlated Molecular Calculations. I. The Atoms Boron Through Neon and Hydrogen *J. Chem. Phys.*, 90 (1989) 1007.
- [61] F. Weigend, F. Furche, R. Ahlrichs, Gaussian Basis Sets of Quadruple Zeta Valence Quality for Atoms H-Kr, *J. Chem. Phys.*, 119 (2003) 12753.
- [62] F. Weigend, R. Ahlrichs, Balanced Basis Sets of Split Valence, Triple Zeta Valence and Quadruple Zeta Valence Quality for H to Rn: Design and Assessment of Accuracy, *Phys. Chem. Chem. Phys.*, 7 (2005) 3297-3305.
- [63] S.F. Boys, F. Bernardi, The Calculation of Small Molecular Interactions by the Differences of Separate Total Energies. Some Procedures With Reduced Errors, *Mol. Phys.*, 19 (1970) 553-566.
- [64] I.V. Yudanov, M. Metzner, A. Genest, N. Rösch, Size-dependence of adsorption properties of metal nanoparticles_a DFT study on palladium nanoclusters, *J. Phys. Chem. C*, 112 (2008) 20269-20275.
- [65] H.J. Monkhorst, J.D. Pack, SPECIAL POINTS FOR BRILLOUIN-ZONE INTEGRATIONS, *Phys. Rev. B*, 13 (1976) 5188-5192.
- [66] G. Kresse, J. Furthmüller, Efficient iterative schemes for ab initio total-energy calculations using a plane-wave basis set, *Phys. Rev. B*, 54 (1996) 11169-11186.
- [67] G. Kresse, J. Hafner, ABINITIO MOLECULAR-DYNAMICS FOR LIQUID-METALS, *Phys. Rev. B*, 47 (1993) 558-561.
- [68] J.P. Perdew, K. Burke, M. Ernzerhof, Generalized Gradient Approximation Made Simple *Phys. Rev. Lett.*, 77 (1996) 3865-3868.
- [69] G. Kresse, D. Joubert, From Ultrasoft Pseudopotentials to the Projector Augmented-Wave Method, *Phys. Rev. B*, 59 (1999) 1758.
- [70] P.E. Blöchl, Projector Augmented-Wave Method, *Phys. Rev. B*, 50 (1994) 17953.
- [71] J. Paier, M. Marsman, G. Kresse, Why does the B3LYP hybrid functional fail for metals?, *The Journal of chemical physics*, 127 (2007) 024103.
- [72] K. Mogi, Y. Sakai, T. Sonoda, Q. Xu, Y. Souma, Geometries and Electronic Structures of Group 10 and 11 Metal Carbonyl Cations, $[M(CO)_n]^{x+}$ ($Mx+ = Ni^{2+}, Pd^{2+}, Pt^{2+}, Cu^+, Ag^+, Au^+$; $n = 1-4$), *The Journal of Physical Chemistry A*, 107 (2003) 3812-3821.
- [73] P.C. Gravelle, Heat-Flow Microcalorimetry and Its Application to Heterogeneous Catalysis, *Adv. Catal.*, 22 (1972) 191.

- [74] P.C. Gravelle, CALORIMETRY IN ADSORPTION AND HETEROGENEOUS CATALYSIS STUDIES, Catal. Rev. Sci. Eng., 16 (1977) 37.
- [75] G. Zanti, D. Peeters, DFT Study of Small Palladium Clusters Pd_n and Their Interaction with a CO Ligand (n= 1-9), Eur. J. Inorg. Chem., (2009) 3904-3911.
- [76] D. Dai, K. Balasubramanian, ELECTRONIC-STRUCTURES OF Pd-4 AND Pt-4 J. Chem. Phys., 103 (1995) 648-655.
- [77] G. Blyholder, Molecular orbital view of chemisorbed carbon monoxide, J. Phys. Chem., 68 (1964) 2772-2777.
- [78] P. Gruene, A. Fielicke, G. Meijer, D.M. Rayner, The adsorption of CO on group 10 (Ni, Pd, Pt) transition-metal clusters, Physical Chemistry Chemical Physics, 10 (2008) 6144-6149.
- [79] T. Komeda, Y. Kim, M. Kawai, Lateral Motion of Adsorbate Induced by Vibrational Mode Excitation With Inelastic Tunneling Electron, Surf. Sci., 502-503 (2002) 12-17.
- [80] K.L. Wong, B.V. Rao, G. Pawin, E. Ulin-Avila, L. Bartels, Coverage and Nearest-Neighbor Dependence of Adsorbate Diffusion, J. Chem. Phys., 123 (2005) 201102.
- [81] M. Peter, S. Adamovsky, J.M. Flores Camacho, S. Schauermaun, Energetics of Elementary Reaction Steps Relevant for CO Oxidation: CO and O₂ Adsorption on Model Pd Nanoparticles and Pd(111), Faraday Discuss., 162 (2013) 341-354.
- [82] H. Unterhalt, G. Rupprechter, H.-J. Freund, Vibrational Sum Frequency Spectroscopy on Pd(111) and Supported Pd Nanoparticles: CO Adsorption from Ultrahigh Vacuum to Atmospheric Pressure, J. Phys. Chem. B, 106 (2001) 356-367.
- [83] S. Bertarione, D. Scarano, A. Zecchina, V. Johánek, J. Hoffmann, S. Schauermaun, M.M. Frank, J. Libuda, G. Rupprechter, H.-J. Freund, Surface Reactivity of Pd Nanoparticles Supported on Polycrystalline Substrates As Compared to Thin Film Model Catalysts: Infrared Study of CO Adsorption, J. Phys. Chem. B, 108 (2004) 3603-3613.
- [84] T. Lear, R. Marshall, E.K. Gibson, T. Schutt, T.M. Klapotke, G. Rupprechter, H.-J. Freund, J.M. Winfield, D. Lennon, A Model High Surface Area Alumina-Supported Palladium Catalyst, Phys. Chem. Chem. Phys., 7 (2005) 565-567.
- [85] M. Scheffler, The Influence of Lateral Interactions on the Vibrational Spectrum of Adsorbed CO, Surf. Sci., 81 (1979) 562-570.
- [86] K. Wolter, O. Seiferth, H. Kuhlbeck, M. Baumer, H.-J. Freund, Infrared Spectroscopic Investigation of CO Adsorbed on Pd Aggregates Deposited on Alumina Model Support, Surf. Sci., 399 (1998) 190-198.
- [87] W.K. Kuhn, J. Szanyi, D.W. Goodman, CO Adsorption on Pd(111): the Effects of Temperature and Pressure, Surf. Sci. Lett., 274 (1992) L611-L618.
- [88] S. Zou, I. Villegas, C. Stuhlmann, M.J. Weaver, Nanoscale Phenomena in Surface Electrochemistry: Some Insights from Scanning Tunneling Microscopy and Infrared Spectroscopy, Electrochim. Acta, 43 (1998) 2811-2824.
- [89] P.S. Bagus, C.J. Nelin, C.W. Bauschlicher, BONDING OF CO TO METAL-SURFACES - A NEW INTERPRETATION, Physical Review B, 28 (1983) 5423-5438.
- [90] T.O. Mentes, N. Stojić, N. Binggeli, M.A. Niño, A. Locatelli, L. Aballe, M. Kiskinova, E. Bauer, Strain Relaxation in Small Adsorbate Islands: O on W(110), Phys. Rev. B, 77 (2008) 155414.
- [91] V. Kumar, Y. Kawazoe, Icosahedral Growth, Magnetic Behavior, and Adsorbate-Induced Metal-Nonmetal Transition in Palladium Clusters, Phys. Rev. B, 66 (2002) 144413.
- [92] M. Mavrikakis, B. Hammer, J.K. Nørskov, Effect of Strain on the Reactivity of Metal Surfaces, Phys. Rev. Lett., 81 (1998) 2819-2822.

Table of Content – Graphic

